JOURNAL OF MATERIALS SCIENCE **34** (1999) 821–826

# The rate-controlling mechanism(s) during plastic deformation of polycrystalline NaCl at 0.28–0.75 $T_M$

HANS CONRAD, DI YANG
*Materials Science and Engineering Department, North Carolina State University, Raleigh, NC 27695-7907*

The plastic deformation kinetics of polycrystalline 99.9% NaCl were determined in compression at 23–532 °C (0.28–0.75$T_M$) and a strain rate $\dot{\varepsilon} = 8.3 \times 10^{-4}$ s$^{-1}$. The rate-controlling mechanism at 0.28–0.65 $T_M$ ($\sigma/\mu > 3 \times 10^{-4}$) was deduced to be the intersection of forest dislocations with a Helmholtz free energy $\Delta F^* = 113$ kJ/mol (0.16 $\mu b^3$). The forest dislocation obstacles become ineffective at ~0.65$T_M$. The kinetics at 0.75$T_M$ ($\sigma/\mu < 3 \times 10^{-4}$) were in accord with the Weertman-Dorn creep equation. At $T < 0.5\ T_M$ the decrease in strain hardening with strain and temperature was attributed to cross slip, leading to a brittle-to-ductile transition at 0.5 $T_M$. Dislocation climb was deduced to become more important at higher temperatures. The stress-strain curves were described reasonably well by the Bergström-Roberts dislocation multiplication model. 

## 1. Introduction

An excellent review of the plastic deformation kinetics of the alkali halides is given by Haasen [1]. The major slip systems are {110} ⟨110⟩ and {100} ⟨110⟩, the critical resolved shear stress (CRSS) for the former generally being smaller than the latter. According to Haasen, the available data indicate that the effect of temperature on the CRSS for the two slip systems has the four regimes shown in Fig. 1. In Regime I overcoming the Peierls-Nabarro stress is concluded to be the rate-controlling mechanism, while Regimes II and III are attributed to the interaction of dislocations with impurity metal ion-vacancy ($M^{++}V^{-}$) dipoles. Regime III ultimately decays in Regime IV to a basic dislocation interaction stress $\tau_\mu$. The stress-strain curves of halide single crystals exhibit three stages similar to the FCC metals. Considerable point defects and dislocation debris are generated in Stages I and II, which is followed by cross slip in Stage III. The degree and extent of cross slip increases with temperature leading to a brittle-to-ductile transition in polycrystals at ~0.5 $T_M$. At $T >$ ~0.5 $T_M$ the climb of dislocations becomes important in both single and polycrystalline specimens.

Although there is some support for the specific rate-controlling mechanisms given by Haasen [1] for each of the Regimes in Fig. 1, other mechanisms have also been proposed. For example, Argon and Padaware [2] conclude from their experimental results that the intersection of forest dislocations is rate controlling during {110} glide in NaCl single crystals at 77–295 K (Regimes I and II). Further, Appel [3] concludes from his measurements on single crystals of NaCl at 210–320 K that dislocation-impurity interactions are rate-controlling at small strains but that the intersection of forest dislocations becomes rate controlling at larger strains, the transition strain decreasing with increase in purity level of the material.

Most studies on the rate-controlling mechanism during the plastic deformation of NaCl have been on single crystals; only little have been done on polycrystals. The objective of the present investigation was therefore to determine the plastic deformation kinetics and identify the rate-controlling mechanism(s) for 99.9% polycrystalline NaCl at 23–532 °C (0.28–0.75 $T_M$), comparing the results with those previously reported for single and polycrystalline specimens. The chosen temperature range is expected to represent Regimes II to IV in Fig. 1. To the authors' knowledge no studies of the plastic deformation kinetics of *polycrystalline* NaCl have previously been made covering these regimes.

## 2. Experimental

Compression tests were conducted on water-polished, as-cast cylinders (2 cm dia. × 5 cm high) of 99.9% NaCl with 2 mm average grain size and the following composition in wt%: 0.001 Ba; 0.003 Br; 0.002 Ca, $MO_2$, $R_2O_3$; 0.006 $NO_3$; 0.0004 I; 0.0003 N; 0.001 K; 0.0008 $SO_4$; 0.5 ppm Fe; 1 ppm $PO_4$; and 0.001 in soluble matter. The tests were performed with an Instron machine at 23 to 693 °C ± 2° (0.28–0.90 $T_M$) in air at an initial strain rate $\dot{\varepsilon} = 8.3 \times 10^{-5}$ s$^{-1}$. Two types of tests were carried out: (a) constant strain rate $\dot{\varepsilon}$ throughout the test and (b) strain rate cycling, whereby the crosshead speed was alternately increased

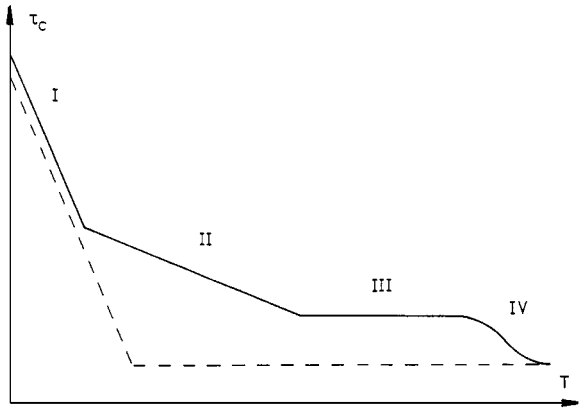


*Figure 1* Schematic of the yield stress vs. temperature for alkali halides: - - - - pure, —— doped. After Haasen [1].

and decreased by a factor of 10 during the test. The $\dot{\varepsilon}$-cycling tests provided values for the *apparent* activation volume

$$v = kT\ell n(\dot{\varepsilon}_2/\dot{\varepsilon}_1)/(\sigma_2 - \sigma_1) \quad (1)$$

and the stress exponent

$$n = \ell n(\dot{x}_2/\dot{x}_1)/\ell n(P_2/P_1) \quad (2)$$

where $P_2$ is the load immediately following and $P_1$ that immediately preceding an increase in crosshead speed from $\dot{x}_1$ to $\dot{x}_2$. $\sigma$ and $\dot{\varepsilon}$ are the respective stresses and strain rates and $kT$ has its usual meaning. The $\varepsilon$-cycling tests were only conducted at 23 to 532 °C (0.28–0.75 $T_M$). The values of $v$ and $n$ for the decreases in strain rate tended to be slightly lower than for the increases.

## 3. Results

The effect of temperature on the true stress $\sigma$ vs. true strain $\varepsilon$ curves are shown in Fig. 2a. The curves are in general accord with those on polycrystalline NaCl of similar purity and grain size in the literature [5–9]. With increase in temperature the flow stress $\sigma$ and the strain hardening rate $\mathrm{d}\sigma/\mathrm{d}\varepsilon$ decrease and the fracture strain $\varepsilon_F$ increases. Plots of $\sigma$ at various strain levels vs. $T/T_M$ in Fig. 2b reveal a sharp change in slope ($\mathrm{d}\sigma/\mathrm{d}T$) at 0.45–0.5 $T_M$, the defining temperature tending to increase with strain level. Associated with the change in slope is a rapid increase in the fracture strain with temperature, representing a brittle-to-ductile transition. The present brittle-to-ductile transition temperature of ~0.5 $T_M$ is in accord with that reported by a number of investigators [1, 4, 6, 7].

The variation of the apparent activation volume $v$ with strain is shown in Fig. 3. Only the average of the values for the increase and decrease in strain rate are plotted to avoid overlapping data points. The values of $v$ range from $6.3 \times 10^{-26}$ m$^3$ (~$10^3$ b$^3$) at small strains to $0.6 \times 10^{-26}$ m$^3$ (~$10^2$ b$^3$) at large strains, decreasing with temperature in the range 23 °C to 371 °C and then increasing slightly at 532 °C. Similar values of $v$ at 23 °C were derived from data in the literature pertaining

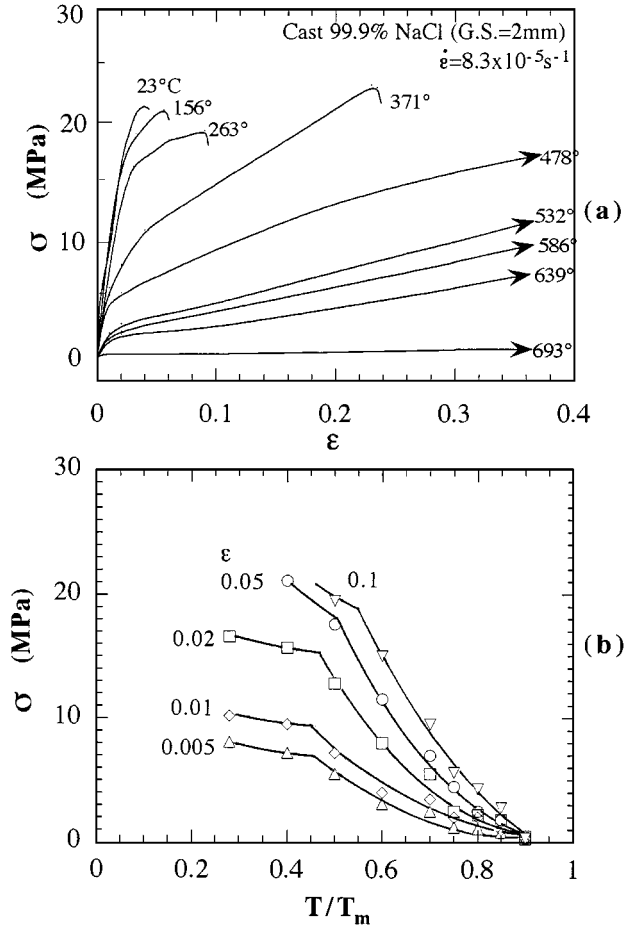


*Figure 2* (a) Effect of temperature on the stress-strain curves and (b) the flow stress at various strains vs. the ratio of test temperature to melting temperature.

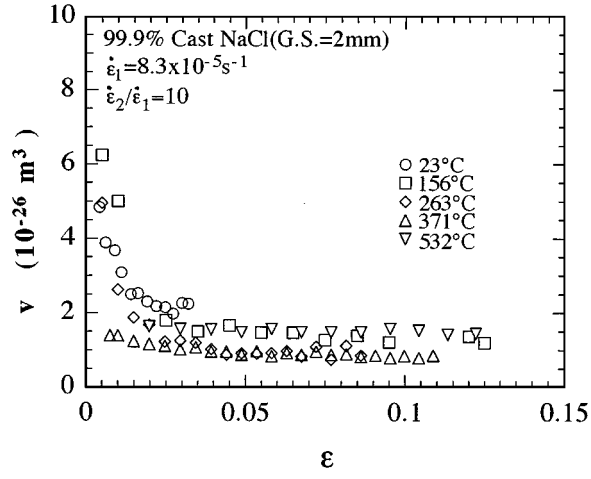


*Figure 3* Variation of the apparent activation volume $v$ with strain at 23–532 °C.

to the effect of strain rate on the flow stress for {110} ⟨110⟩ glide in NaCl single crystals [2, 3, 8–13]. Fig. 4 shows that the variation of $v$ with strain corresponds to a proportionality between $1/v$ and the flow stress $\sigma$, the proportionality constant increasing with temperature.

The variation of the stress exponent $n$ given by Equation 2 with strain and temperature is presented in Fig. 5. $n$ is relatively independent of strain at each temperature, but decreases with temperature from a value of ~80 at 23 °C to 4 at 532 °C. The behavior of $n$ is in

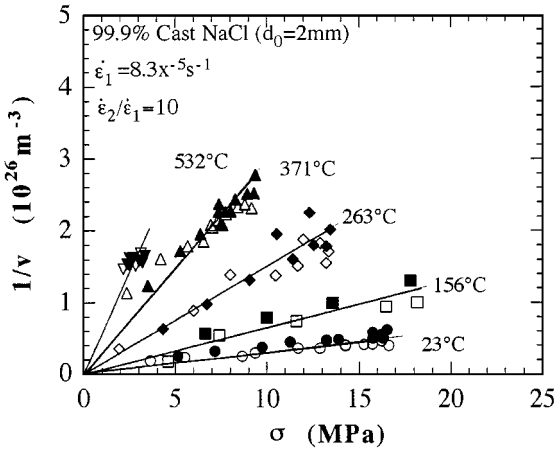


*Figure 4* $1/v$ vs. the applied stress at the various temperatures. Open data points are for increases in strain rate; filled are for decreases.

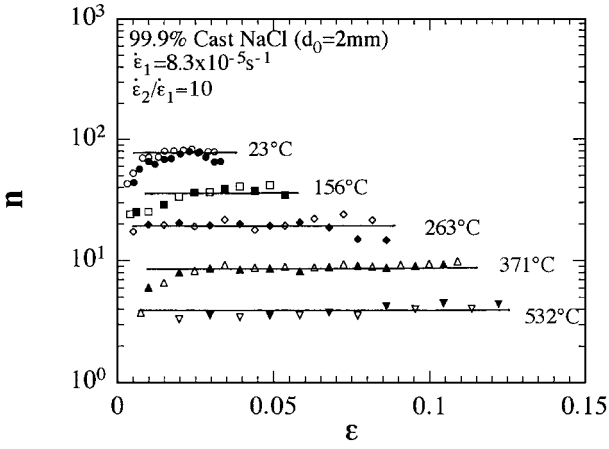


*Figure 5* Stress exponent $n$ vs. strain at various temperatures. Open data points are for increases in strain rate; filled are for decreases.

accord with the dependence of $v$ on stress and temperature shown in Fig. 4, in that $n = v\sigma/kT$.

## 4. Discussion

In keeping with the behavior of crystalline solids in general the plastic deformation kinetics of NaCl single and polycrystals at elevated temperatures exhibits two regimes [14–16]: (a) when $\sigma/\mu < \sim 3 \times 10^{-4}$ ($\mu$ is the shear modulus), the dependence of the strain rate on the stress obeys a power law with the stress exponent $n = 4$–6 and the kinetics are given by the well-known Weertman-Dorn creep equation and (b) when $\sigma/\mu > \sim 3 \times 10^{-4}$ the dependence of the strain rate on the stress is given by an exponential stress law, i.e., with $\dot{\varepsilon} \propto \exp B\sigma$. It is generally accepted that the rate-controlling mechanism in the power law regime is the glide and climb of dislocations [17]; that in the exponential law regime has yet to be unambiguously defined. Except for the lowest stresses at 532 °C, the present results all fall within the exponential stress law regime, in that $\sigma/\mu > 3 \times 10^{-4}$ ($\mu = 1.8 \times 10^4 - 10.23T$ (MPa) [15]) and/or $n > 6$. Since the major deformation mode in this regime is {110} ⟨110⟩ glide [5, 14, 15], it is expected that the present plastic deformation kinetics refer to dislocation glide on this system. Of interest then is the rate-controlling mechanism(s) which governs the kinetics pertaining to this glide system in the temperature range of the present tests.

Thermally activated overcoming of short-range obstacles to dislocation motion is given by the following relations [18]

$$\dot{\varepsilon} = \dot{\varepsilon}_0 \exp -(\Delta G/kT) \tag{3}$$

$$\Delta G = \Delta F^* - v^*\tau^* = \Delta H^* - T\Delta S^* \tag{4}$$

with

$$\dot{\varepsilon}_0 = \frac{\rho_m A b \nu}{M\ell^*} \tag{5}$$

where $\Delta G$ is the Gibbs free energy of activation, $\Delta F^*$ the Helmhotz free energy, $\Delta S^*$ the activation entropy, $v^* = \ell^* b x^*$ the *true* activation volume (with $\ell^*$ the spacing between obstacles and $x^*$ the activation distance) and $\tau^* = \sigma^*/M$ the resolved effective shear stress. $\dot{\varepsilon}_0$ is the pre-exponential, $M$ the Taylor orientation factor, $\rho_m$ the mobile dislocation density, $A \approx (\ell^*)^2$ the area swept out per successful thermal fluctuation, $b$ the Burgers vector, $\nu = (b/\ell^*)\nu_D$ the attack frequency (with $\nu_D$ the Debye frequency). Inserting Equation 4 into Equation 3 and rearranging one obtains

$$v^*\tau^* = \Delta F^* - kT\ell n(\dot{\varepsilon}_0/\dot{\varepsilon}) \tag{6}$$

The linear increase of $1/v$ with the flow stress in Fig. 3 indicates a scaling between the short-range and long-range obstacles to dislocation motion, i.e. a proportionality between the thermal component of the flow stress $\sigma^*$ (effective stress) and the athermal component $\sigma_\mu$, where the total flow stress is given by

$$\sigma = \sigma^* + \sigma_\mu \tag{7}$$

The scaling between the short-range and long-range obstacles gives

$$\tau^* \approx \alpha_1 \tau = \alpha_1 \sigma/M \tag{8}$$

A reasonable value for $\alpha_1$ in our polycrystalline NaCl is 0.25 [2, 3]. For discrete obstacles [18, 19]

$$v^* = \frac{3}{2} M v \approx \ell^* b^2 \tag{9}$$

Substituting Equations 8 and 9 into Equation 6 gives

$$v\sigma = \frac{2\Delta F^*}{3\alpha_1} - \frac{2}{3\alpha_1} kT\ell n(\dot{\varepsilon}_0/\dot{\varepsilon}) \tag{10}$$

Hence, a plot of the product $v\sigma$ ($= nkT$) vs. temperature should give a straight line with intercept on the ordinate $2\Delta F_0^*/3\alpha_1$ and with slope $(2k/3\alpha_1)$ $\ln(\dot{\varepsilon}_0/\dot{\varepsilon})$. Fig. 6 presents such a plot, which is in accord with Equation 10. Taking $\alpha_1 = 0.25$ one obtains $\Delta F^* = 113$ kJ/mol ($0.16\,\mu_0 b^3$) from the intercept and $\dot{\varepsilon}_0 = 2.3 \times 10^4\ \mathrm{s}^{-1}$ from the slope. Further, taking $\nu_D = 10^{13}\ \mathrm{s}^{-1}$, $b = 4 \times 10^{-10}$ m and $M = 2$, Equation 4

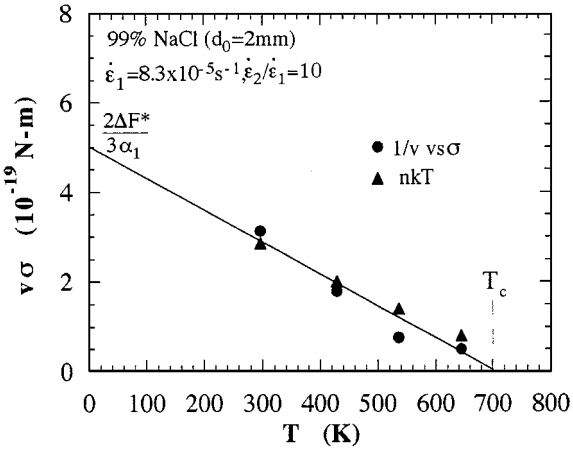


*Figure 6* The products $v\sigma$ and $nkT$ vs. temperature.

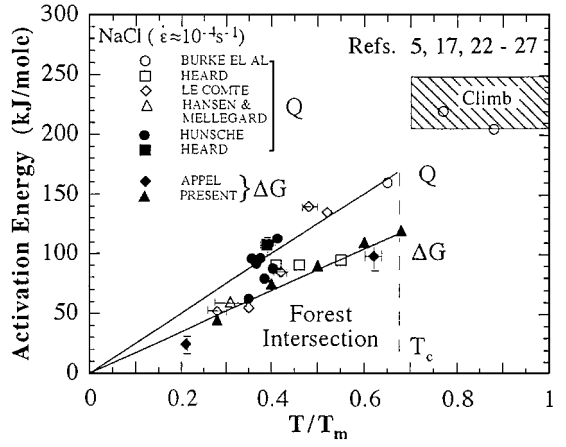


*Figure 7* Activation energy vs. $T/T_M$ for present tests and from data in the literature [3, 5, 15, 17, 23–27].

gives $\rho_m = 2.8 \times 10^{10}$ m$^{-2}$. The values of $\Delta F^*$ and $\dot{\varepsilon}_0$ are in accord with those obtained by Appel [3] on NaCl single crystals. The intercept on the abscissa in Fig. 6 gives $T_c = 700$ K (0.65 $T_M$), where thermal fluctuation provide the entire energy for overcoming the obstacles to dislocation motion, i.e. they become ineffective (transparent).

The values of the Gibbs free energy of activation $\Delta G$ derived from the data in Fig. 6 using Equation 4 are plotted vs. $T/T_M$ in Fig. 7. Included are the values of $\Delta G$ for the deformation of NaCl single crystals from Appel [3]† and the values of the apparent activation energy $Q$ obtained by various investigators on NaCl single and polycrystals. Reasonable agreement exists between the present values of $\Delta G$ for polycrystals and those from Appel for single crystals. The higher values of $Q$ obtained by others for single and polycrystalline NaCl compared to $\Delta G$ in the temperature range 0–700 K could be due to one or more of the following reasons: (a) the measurements were made at a lower strain rate, (b) the activation entropy $\Delta S^*$ is not included in $Q$ ($\Delta S^*$ is estimated to be 2–3 K giving $T\Delta S = 12$–17 kJ/mol at $T_c$), (c) $Q$ was not obtained at a constant defect structure and therefore includes an effect of temperature on structure, (d) $Q$ includes the energy to overcome the long-range internal stress and (e) $Q$ includes a contribution from the impurity content. The data in Fig. 7 suggest that one rate-controlling mechanism is dominant from 200 to 700 K with $\Delta F^* = 113$ kJ/mol and another at higher temperatures with $\Delta H \approx 210$ kJ/mol.

† The values of $\Delta G(\tau^* = 0) = \Delta F^*$ at $T = T_c$ given for Appel in Fig. 6 were obtained by making the correction that the true activation volume $v^* = 3/2kT\ \partial \ell n\dot{\gamma}/\partial\tau$ in his derivation of $\Delta F^*$. This correction is based on Friedel's equation $\ell^* = (2\mu b/N\tau^*)^{1/3}$ due to the bowing of dislocations [18, 19], where $N$ is the obstacle density.

TABLE I Dislocation densities in units of $10^{12}$ m$^{-2}$

| T °C | $\varepsilon$ | $\sigma$ MPa | $\rho_f^{v(1)}$ | $\rho_f^{(2)}$ (Predicted) | $\rho_s^{(3)}$ (Measured) | $\rho_t^{(4)}$ |
|---|---|---|---|---|---|---|
| 23 | 0.03 | 18 | 28 | 25 | 16 | 50 |
| 371 | 0.03 | 3 | 7 | 2 | 1 | 3 |

(1) $\rho_f^v$ (forest) $= (1/\ell^*)^2 = (2b^2/3Mv)^2$ [Eqn. 9 in text]
(2) $\rho_f$ (forest) $= (\sigma/0.3\ M\mu b)^2$ [21]
(3) $\rho_s$ (secondary) $= (\sigma/0.37\ M\mu b)^2$ [21]
(4) $\rho_t$ (total) $= (\sigma/0.21\ M\mu b)^2$ [Eqn. 15 in text]

The scaling between the thermal and athermal components of the flow stress at $T \leq 700$ K in the present tests suggests that the intersection of forest dislocations is the rate-controlling mechanism [18]. Also, the magnitude of $\Delta F^*$, is in qualitative accord with the energy to form a jog [20]. Furthermore, the forest dislocation densities derived from the values of the apparent activation volume are in reasonable accord with theoretical predictions and experimental measurements on NaCl [3, 21, 22]; see Table I. These results provide strong support that the dominant rate-controlling mechanism in our *polycrystalline* NaCl at 23 to 427 °C (0.28–0.65 $T_M$) is the intersection of forest dislocations by dislocations gliding on {110} planes. This is in accord with the conclusion reached by Appel [3] for significant straining of NaCl *single* crystals at room temperature and below. Overcoming cation impurity-vacancy dipoles was deduced by him to be rate-controlling only at small strains, and became ineffective at $T_c \geq 313$ K (0.29 $T_M$).

The intersection of the line in Fig. 6 with the abscissa at $T = 427$ °C indicates that the forest dislocation become ineffective (transparent) obstacles at this temperature and that another mechanism becomes rate-controlling at higher temperatures. The value of the stress exponent $n = 4$ at 532 °C (0.75 $T_M$) obtained in the present tests is in accord with the dislocation glide and climb mechanism given by the well-known Weertman-Dorn (W-D) equation

$$\dot{\varepsilon} = \frac{A\mu b}{kT} D_\ell \left(\frac{\sigma}{\mu}\right)^n \tag{11}$$

where $A$ is a constant, $D_\ell = D_0 \exp(-\Delta H_\ell/kT)$ the lattice diffusion coefficient and $n = 4$–6. Taking the climb process to be governed by anion diffusion with $D_\ell = 2.5 \times 10^{-2} \exp(-217\ \text{kJ/mol}/kT)$ [17], the present results yield $A = 5 \times 10^7$ for this constant in the W-D equation. Although this value of $A$ is larger than that given for NaCl in [17], it is in accord with that frequently obtained for glide and climb, suggesting that this mechanism is rate-controlling at 532 °C. That the climb of dislocations is rate controlling in NaCl at $T > 450$ °C is supported by the magnitude of $Q$ (205–250 kJ/mol) obtained by others [5, 17, 23–27], which is shown by the shaded area in Fig. 7.

It is seen in Fig. 2 that strain hardening occurred at all temperatures except 693 °C (0.9 $T_M$), with its rate, $d\sigma/d\varepsilon$, decreasing with temperature. $d\sigma/d\varepsilon$ can be considered to consist of three components

$$\frac{d\sigma}{d\varepsilon} = \left(\frac{d\sigma}{d\varepsilon}\right)_{II} - \left(\frac{d\sigma}{d\varepsilon}\right)_{cs} - \left(\frac{d\sigma}{d\varepsilon}\right)_{cl} \qquad (12)$$

where $(d\sigma/d\varepsilon)_{II}$ is equivalent to Stage II hardening in single crystals ($\sim 10^{-2}\mu$), $-(d\sigma/d\varepsilon)_{cs}$ recovery due to cross slip and $-(d\sigma/d\varepsilon)_{cl}$ recovery due to climb. The kinetics for cross slip in NaCl single crystals is given by [1]

$$\dot{\varepsilon} = \dot{\varepsilon}_0 \exp -[Q_{cs}(\tau)/kT] \qquad (13)$$

where $\dot{\varepsilon}_0 = \rho_m \nu b \ell \approx 10^8$ s$^{-1}$ with $\rho_m$ the mobile dislocation density, $\nu$ the attack frequency, $b$ the Burgers vector and $\ell$ the dislocation segment path length. $Q_{cs}(\tau)$ is the activation energy, which is given by

$$Q_{cs}(\tau) = -A, \ell n\left[(\tau_{III}/\mu_0)/(\tau^0_{III}/\mu_0)\right] \qquad (14)$$

where $A = 0.16 \pm 0.3$ eV for NaCl, $\tau^0_{III}$ the resolved shear stress for cross slip at temperature $T$, $\tau^0_{III}$ that at 0 K and $\mu$ and $\mu_0$ the respective shear moduli. For temperatures below 227 °C (0.47 $T_M$), $Q_{cs}$ was found to be 0.5 eV (117 kJ/mol) [23]. Since the activation energy for anion diffusion-controlled dislocation climb is $Q_c = 217$ kJ/mol [17], the lower value of $Q_{cs}$ suggests that cross slip is the major recovery mechanism in the present tests at $T \leq 0.5\ T_M$, giving the brittle-to-ductile transition $T_{bd}$ observed here at $\sim 0.5\ T_M$. Fig. 8 shows that $T_{bd}$ for the present polycrystals is in accord with measurements of $T_{bd}$ and $T_w$ (where {110} slip lines become wavy already at the beginning of deformation) and with calculations of the temperature where $\tau_{III}(T) = \tau_0(T)$ the resolved yield stress at temperature $T$ [23].

At $T > 0.5\ T_M$ dislocation climb becomes more and more important as the recovery mechanism. At

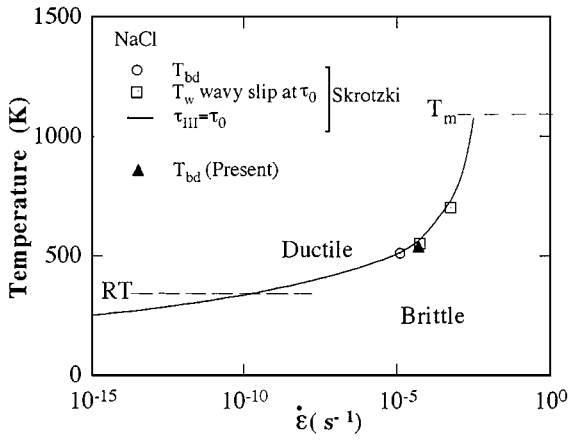


*Figure 8* Dependence on strain rate of: (a) $T_{bd}$, the brittle-to-ductile transition temperature, (b) $T_w$, the temperature at which {110} slip bands become wavy at the beginning of deformation and (c) the temperature where $\tau_{III}$ ($T$) equals the yield stress $\tau_0$ ($T$). Present result and data from Skrotzki [23].

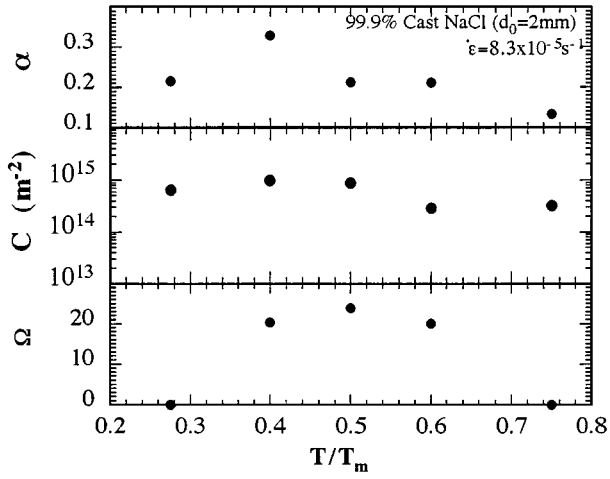


*Figure 9* The parameters $\alpha$, $C$ and $\Omega$ vs. $T/T_M$ derived from the stress-strain curves employing the Bergström-Roberts model.

$T \approx 0.65\ T_M$ ($\dot{\varepsilon} \approx 10^{-4}$ s$^{-1}$) the forest dislocations become ineffective and dislocation climb controlled by anion diffusion becomes the dominant rate-controlling mechanism.

Finally of interest is a description of the stress-strain curves of NaCl in terms of the dislocation multiplication model of Bergström and Roberts [28–30], which gives

$$\sigma = M\alpha\mu b\rho_t^{1/2} \qquad (15)$$

$$\sigma = M\alpha\mu b\left\{\frac{C}{\Omega}[1 - \exp(1 - \Omega\varepsilon)] + \rho_0 \exp(-\Omega\varepsilon)\right\}^{1/2} \qquad (16)$$

where $\rho_t$ is the total dislocation density, $C$ is the rate of immobilization of mobile dislocations, $\Omega$ the probability of remobilization of immobile dislocations and $\rho_0$ the initial dislocation density. Taking $M = 2$ and the reasonable value $\rho_0 = 10^{10}$ m$^{-2}$ [3, 5, 15], the parameters $\alpha$, $C$ and $\Omega$ were determined by a fit of the stress-strain curves in Fig. 2a to Equation 16 using a computer. The values so obtained are plotted vs. $T/T_M$ in Fig. 9. It is noted that $\alpha \approx 0.2$, $C \approx 10^{15}$ m$^{-2}$ and $\Omega = 0$ to 20 with a tendency for all parameters to decrease at $T/T_M = 0.75$ (532 °C). The parameters $\alpha$ and $C$ are in accord with those obtained for metals in general [30]; however the value of $\Omega = 20$ is somewhat higher, e.g., compared to 3.5–4.0 for the high stacking fault metal Al [30, 31]. Of significance is that the total dislocation density $\rho_t$ determined using the above values of $\alpha$ is in accord with the values for the density of forest dislocations derived from measurements of the activation volume in the present polycrystals and measurements of the density of secondary dislocations in single crystals [21]; see Table I.

## 5. Summary and conclusions

1. The plastic deformation kinetics of large grain size ($d = 2$ mm) polycrystalline 99.9% NaCl were determined in compression at 23–532 °C (0.28–0.75 $T_M$) and strain rate $\dot{\varepsilon} = 8.3 \times 10^{-5}$ s$^{-1}$.

2. The rate-controlling mechanism at 0.28–0.65 $T_M$ ($\sigma/\mu > 3 \times 10^{-4}$) is the intersection of forest

dislocations by gliding {110} ⟨110⟩ dislocations, giving a Helmholtz free energy $\Delta F^* = 113$ kJ/mol ($0.16\ \mu_0 b^3$). The forest dislocation obstacles became ineffective at 427 °C ($0.65\ T_M$).

3. The dislocation forest densities determined from the apparent activation volume measurements were in accord with theoretical predictions and measurements given in the literature.

4. At $T < 0.5\ T_M$ cross slip of screw dislocations was the dominant recovery mechanism which reduced strain hardening, leading to a ductile-to-brittle transition at $\sim 0.5\ T_M$. Climb of edge dislocations became important as a recovery mechanism at higher temperatures.

5. The rate-controlling mechanism for $T = 0.75\ T_M$ ($\sigma/\mu < 3 \times 10^{-4}$) was deduced to be glide and climb controlled by anion diffusion.

6. The total dislocation density derived by fitting the stress-strain curves to the Bergström-Roberts dislocation multiplication model was in accord with the dislocation densities determined from the present activation volume measurements and reported dislocation densities in deformed NaCl single crystals.

## Acknowledgement

This research was sponsored by the U.S. Army Research Office under Grant No. DAAH04-94G-0311 with Dr. W. Simmons as technical monitor.

## References

1. P. HAASEN, "Dislocations and Properties of Real Materials" (The Institute of Metals, London, 1985) p. 312.
2. A. ARGON and G. PADAWER, *Phil. Mag.* **25** (1972) 1073.
3. A. APEL, *Phys. Stat. Sol. (a)* **25** (1974) 607; **31** (1975) 617.
4. R. J. STOKES, *Proc. Br. Ceram. Soc.* **6** (1966) 189.
5. H. C. HEARD, "Flow and Fracture of Rocks," Geophysical Monograph 16 (American Geophysical Union, Washington, DC, 1972) p. 191.
6. N. STOLOFF, D. LEZIUS and T. L. JOHNSTON, *J. Appl. Phys.* **34** (1963) 3315.
7. W. SKROTSKI and P. HAASEN, in "Deformation Ceramic Materials," edited by R. Tessler and R. Bradt (Plenum Press, New York, 1984) p. 429.
8. R. W. DAVIDGE and P. L. PRATT, *Phys. Stat. Sol.* **6** (1964) 759.
9. A. G. EVANS and P. L. PRATT, *Phil. Mag.* **21** (1970) 951.
10. S. KOMMIK, V. BENGUS and E. D. LYAK, *Phys. Stat. Sol.* **19** (1967) 5334.
11. L. B. ZUEV, V. GORMOV, A. NAROZHNYI and O. TARSEV, *Sov. Phys. Solid State* **16** (1974) 302.
12. T. SUZUKI and H. KIM, *J. Phys. Soc. Japan* **10** (1976) 1703.
13. O. K. TARSEV, A. N. NAROZHNYI, L. B. ZUEV and S. A. DATSUK, *Problemy Prochnosti*, **1** (1977) p. 111.
14. N. L. CARTER and H. C. HEARD, *Amer. J. Sci.* **269** (1970) 193.
15. S. V. RAJ and G. M. PHARR, *Mater. Sci. Eng.* **A122** (1989) 233.
16. M. C. TSENN and N. L. CARTER, *Scripta Met. Mater.* **23** (1990) 1115.
17. H. J. FROST and M. F. ASHBY, "Deformation Mechanism Maps" (Pergamon Press, New York, 1982) pp. 75–78.
18. U. F. KOCKS, A. S. ARGON and M. F. ASHBY, *Prog. Mater. Sci.* **19** (1975) 1.
19. H. CONRAD, B. de MEESTER, C. YIN and M. DONER, in "Rate Processes in Plastic Deformation of Materials," edited by J. C. M. Li and A. K. Mukherjee (ASM, Metals Park, OH, 1975) 175.
20. A. SEEGER, "Handbook of Physics," (Springer-Verlag VII **12** 114 (1958).
21. H. STRUNK, *Mater. Sci. Eng.* **27** (1977) 225.
22. L. KEMTER and H. STRUNK, *Phys. Stat. Sol. (a)* **40** (1977) 385.
23. W. SKROTZKI, "The Mechanical Behavior of Salt" (Trans. Tech. Publications, Claus-Zellerfeld, Germany, 1984) p. 381.
24. D. E. MUNSON and P. R. DAWSON, *ibid.*, p. 717.
25. U. HUNSCHE, *ibid.*, p. 159.
26. B. ILSCHNER and B. REPPICH, *Phys. Stat. Sol.* **3** (1963) 2093.
27. F. SCHUH, W. BLUM and B. ILSCHNER, *Proc. Brit. Ceram. Soc.* **15** (1970) 143.
28. Y. BERSTROM, *Mater. Sci. Eng.* **5** (1969/70) 193.
29. W. ROBERTS and Y. BERSTROM, *Acta Metall.* **21** (1973) 457.
30. Y. BERSTROM and S. OLUND, *Mater. Sci. Eng.* **56** (1982) 47.
31. A. ZAYED, Y. SHIN and H. CONRAD, in "Aluminum Alloys Their Physical and Mechanical Properties, Vol. III," edited by E. A. Starke and T. H. Sanders (EMAS, Warley, UK, 1986) p. 1691.

*Received 30 October 1997*
*and accepted 8 October 1998*